

Nanotubes

Robust Ordered Bundles of Porous Helical Nanotubes Assembled from Fully Rigid Ionic Benzene-1,3,5-tricarboxamides

Xibo Wu,^[a] Daoliang Wang,^[b] Mingming Chen,^[a] Chengsha Wei,^[c] Shenghui Wei,^[a] Ningdong Huang,^{*[a]} Liangbin Li,^{*[a, c]} and Guobing Zhang^[a]

Abstract: Size-controlled and ordered assemblies of artificial nanotubes are promising for practical applications; however, the supramolecular assembly of such systems remains challenging. A novel strategy is proposed that can be used to reinforce intermolecular noncovalent interactions to construct hierarchical supramolecular structures with fixed sizes and long-range ordering by introducing ionic terminals and fully rigid arms into benzene-1,3,5-tricarboxamide (BTA) molecules. A series of similar BTA molecules with distinct terminal groups and arm lengths are synthesized; all form hexagonal bundles of helical rosette nanotubes spontaneously in water.

Despite differences in molecular packing, the dimensions and bundling of the supramolecular nanotubes show almost identical concentration dependence for all molecules. The similarities of the hierarchical assemblies, which tolerate certain molecular irregularities, can extend to properties such as the void ratio of the nanotubular wall. This is a rational strategy that can be used to achieve supramolecular nanotubes in aqueous environments with precise size and ordering at the same time as allowing molecular modifications for functionality.

Introduction

One-dimensional supramolecular structures such as nanofibers, nanoribbons, and nanotubes with diameters of between 10 and 1000 nm are endowed with unique properties by coupling the merits of supramolecular assemblies and nanometer-scale geometries.^[1] The potential applications of such systems span from the preparation of novel drug-delivery agents to catalytic and photonics materials.^[2] However, their successful application requires control over the self-assembly with regard to size and alignment or ordering between entities.^[1c] Intense research by many groups has focused on investigating the principles that govern supramolecular assembly so that nanoscale tailoring can be achieved.^[1c] For nanoscale systems of meso-

scopic length, control of size and interactions is more subtle than is required for systems of atomic, microscopic, or macroscopic scales. Usually, supramolecular assembly is sensitive to the structural details of block molecules, which hampers simultaneous control of the structure and functionality.

Benzene-1,3,5-tricarboxamide (BTA) molecules with diverse functional arms and unusual self-assembled structure have received increasing attention in recent years.^[3] In contrast to chromonic molecules with simple planar shape^[4] or thermotropic molecules with flexible chains,^[5] BTA molecules with fully rigid arms possess a very diverse range of geometry, functional group distribution, and arm species, which not only facilitate strong intermolecular forces and robust superstructures but also facilitate the regulation of functionalities.^[6] On the other hand, it was recently discovered that introducing charges to the terminal groups of molecules can induce long-range ordering of self-assembled nanofibers.^[7] Therefore, by decorating BTA molecules with ionic terminals, it was anticipated that control over the size and the order of the assemblies could be achieved. Preceding research by our group^[8] on lyotropic phases self-assembled by fully rigid ionic BTA molecules revealed robust hexagonal phases of supramolecular helical nanotubes with tolerance for defects in the peripheral ionic groups for a series of molecules with almost identical structure. The self-organized nanotubes adopt a helical rosette architecture to minimize the electrostatic repulsion among the terminal charges and also to maximize hydrogen bonding between amide groups as well as the π - π interactions between phenyl rings of adjacent molecules. The electrostatic repulsion between charges on the surface of nanotubes also helps the alignment of the nanotubes into ordered bundles. It should be

[a] X. Wu,⁺ M. Chen, S. Wei, Prof. Dr. N. Huang, Prof. Dr. L. Li, Prof. Dr. G. Zhang
National Synchrotron Radiation Lab
and College of Nuclear Science and Technology
University of Science and Technology of China
No 96, JinZhai Road, Hefei, Anhui, 20026 (P.R. China)
Fax: (+86) 551-5141078
E-mail: ndhuang@ustc.edu.cn
lbli@ustc.edu.cn

[b] Dr. D. Wang⁺
Hefei Institute for Public Safety Research and
Tsinghua University (P.R. China)

[c] C. Wei, Prof. Dr. L. Li
CAS Key Laboratory of Soft Matter Chemistry
Department of Polymer Science and Engineering
University of Science and Technology of China (P.R. China)

[⁺] These authors contributed equally to this work.

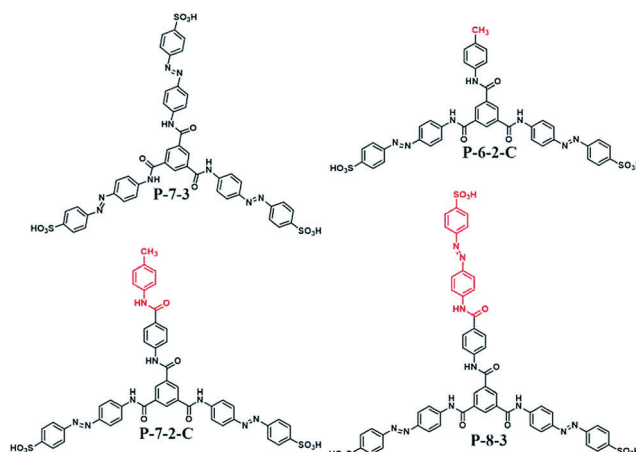
Supporting information for this article is available on the WWW under
<http://dx.doi.org/10.1002/chem.201501422>.

mentioned that hydrophobic effects also contribute to assembly, which usually dominate the dense packing of amphiphiles with flexible chains. However, in the case of ionic BTA molecules with rigid arms, hydrophobic effects are no longer the main driving force. Instead, the assembly is packed much looser (molecules are separated from each other along the azimuth of the rosette walls, resulting in a high void ratio) and is maintained by electrostatic interactions together with hydrogen bonding and π - π interactions.^[8] The synergetic optimization of various noncovalent interplays between the ionic BTA molecules could thus provide new opportunities to obtain organic channels with robust size and long-range ordering on the nanoscale.^[3a,9]

In this work, we demonstrate the robustness of the hierarchical structures assembled by the fully rigid ionic BTA molecules against even more severe irregularities or versatilities of molecular structures than ionic end-groups. New sequences of BTA molecules with similar structures but with varied arm length and functional group distributions are designed and synthesized. The spontaneous supramolecular assemblies of all molecules in aqueous solutions are then investigated by using several experimental techniques including polarizing optical micrographs (POM), small-angle and wide-angle X-ray scattering (SAXS/WAXS), and ultra-violet circular dichroism (UV-CD). Interestingly, it is found that the lyotropic liquid-crystal phases of helical rosette nanotubes are very well preserved for all BTA molecules. Although the stacking of molecules inside the nanotubes does rely on the arm length and ionic termination, the sizes and hexagonal ordering of supramolecular nanotubes depend only on the concentration and not on the molecular details. Model calculations on the void ratio of the porous walls of the nanotubes reveals close values due to compensation between molecular number and arm length. The results demonstrate the ability of the designed BTA molecules to self-adjust and to maintain the architecture as well as certain properties by incorporating electrostatic and other noncovalent interactions. The role of electrostatic repulsion between the charged nanotubes in their ordering as well as the relationship between correlation length inside the bundles and the charges on the nanotubes are also discussed. The supramolecular nanotubular assemblies constructed by relatively simple and robust scaffolds of ionic BTA molecules sheds light on rosette microtubules^[10] with nanoscale structural control for potential applications in systems for which different functionalities can be introduced without disturbing the structures and other properties.

Results and Discussion

Materials, synthetic details, and characterization of all new compounds (Scheme 1) are given in the Supporting Information (Part 1). The molecules are named P- n_1 - n_2 (-C), where n_1 denotes the total number of phenyl rings, n_2 the number of ionic end-groups at the molecular periphery, and the optional finishing letter C denotes the replacement of one ionic terminal by a methyl group. The C_3 symmetric molecule **P-7-3** has been characterized previously^[8] and the data are included here to



Scheme 1. Chemical structures of **P-7-3**, **P-6-2-C**, **P-7-2-C**, and **P-8-3**.

represent the behavior of molecules with perfect symmetry and no irregularities. The other three molecules all surrender the C_3 symmetry by altering the number of phenyl rings along one arm (one less or more ring for **P-6-2-C** or **P-8-3**) or by changing the chemical component of one arm (- SO_3H end-group is replaced by - CH_3 for **P-7-2-C** and **P-6-2-C**) as shown in Scheme 1. In addition, one more amide group is introduced into the defective arm of **P-7-2-C** and **P-8-3** to amplify the distinction between the molecules and the symmetric **P-7-3**.

With increasing concentration, aqueous solutions of all BTA molecules transform from translucent fluids to liquid-crystal (LC) and gel-like states similar to **P-7-3**, as shown for **P-6-2-C** in Figure S1 in the Supporting Information. The lyotropic LC behavior was studied by POM and the data are summarized in Table 1. The three molecules with defects show very similar

Table 1. Phase behavior of aqueous solutions of the full rigid BTA molecules probed by polarizing optical micrographs (POM). The concentration range for each phase was estimated from POM observations for the purpose of reference but not exact phase boundaries.

BTA molecules	P-7-3	P-6-2-C	P-7-2-C	P-8-3
liquid crystal (mol L^{-1})	0.050	0.037	0.021	0.027
gel (mol L^{-1})	0.111	0.085	0.085	0.090

concentration range of the LC phase, whereas the perfectly symmetric **P-7-3** molecule shows higher concentration for LC because of its better solubility. Figure 1 displays typical POM images of the water/BTAs mixtures in the LC phase, which all exhibit similar streak texture, an indication of nematic LC. At higher concentration in the gel-like state, a stripe texture originating from column undulations is observed for aqueous solutions of **P-7-3** and **P-8-3** but not for the other two molecules with fewer charged terminals (see Figure S2 in the Supporting Information). This suggests that the materials have different mesogenic structures, which is also evident in the SAXS data discussed later.

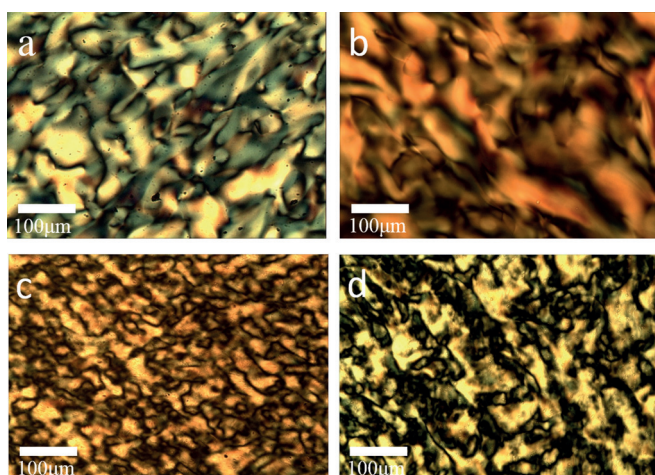


Figure 1. Representative POM of aqueous solutions of BTA molecules in the liquid-crystal phase: a) P-7-3 at 0.050 mol L⁻¹, b) P-6-2-C at 0.037 mol L⁻¹, c) P-7-2-C at 0.021 mol L⁻¹, and d) P-8-3 at 0.027 mol L⁻¹.

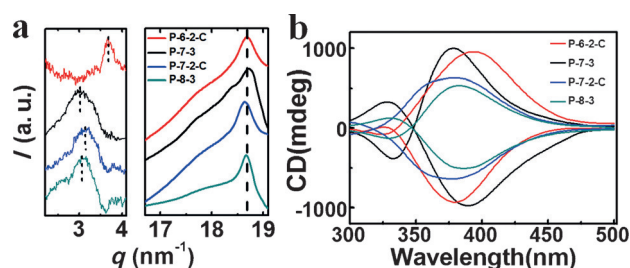


Figure 2. a) WAXS of aqueous solutions of BTA molecules demonstrating similar intermolecular correlation (peaks ca. 18.7 nm⁻¹) because of π - π stacking and signal at lower q between 3 and 4 nm⁻¹ due to helical periodicity. Concentrations of 0.131, 0.159, 0.118, and 0.117 mol L⁻¹ for P-7-3, P-6-2-C, P-7-2-C, and P-8-3, respectively. b) CD spectra showing the existence of chirality in the lyotropic system, consistent with formation of helices by BTAs. The concentration was 0.131, 0.081, 0.053, and 0.045 mol L⁻¹ for P-7-3, P-6-2-C, P-7-2-C, and P-8-3, respectively.

The microscopic structure in the aqueous solutions of the BTA molecules was studied with WAXS and CD; the results are presented in Figure 2. Two major WAXS features are observed in Figure 2a including a prominent peak with a q value of 18.7 nm⁻¹ for all BTA molecules (highlighted by a vertical dashed line) and a weaker signal at smaller q . The former corresponds to real-space periodicity around 0.34 nm, coincident with the distance of π - π stacking between phenyl rings, which only slightly changes for different molecules. The latter is attributed to helical stacking, similar to that found for P-7-3 in the previous work, which remains around 3.1 nm⁻¹ for the other molecules except for P-6-2-C as a result of modified helical pitch due to molecular distinctions. BTA molecules are well known to form columnar, even helical, assemblies through π - π stacking and hydrogen bonding.^[11] In contrast to broad diffused scattering peaks that are usually observed for molecules containing flexible chains because of short-range ordering of molecules,^[12] the pronounced WAXS features here indicate long-range ordering of the fully rigid BTA molecules along the axis of assembled columns in water. Detailed stacking param-

eters, such as rotation of the adjacent molecules as well as the tilt of molecules with respect to the stacking plan, should be altered because these properties are, in general, sensitive to molecular structures. However the WAXS data suggest that all molecules pack into helices, as further supported by CD experiments.

Usually, supramolecular columns that are built from propeller BTA molecules are helices, and macroscopic handedness can be obtained if the molecule itself possesses a certain type of chirality. For achiral building units, chiralities of individual assembled helix are randomly distributed and will cancel each other, resulting in zero macroscopic chirality. However, the CD spectra in Figure 2b show both large positive and negative Cotton effects for all achiral BTA molecules in this study, which was previously attributed to collective chiral symmetry breaking of supramolecular assemblies in a spontaneous but unpredicted fashion. Here, a more conceivable interpretation is offered based on artificial contribution from a partial orientation in the CD spectra of both chiral and achiral assemblies.^[13] The CD experiments were performed with the sample solutions sandwiched between two pieces of slide glass. Partial alignment of helical assemblies may thus be induced by shear during the sample preparation. The orientation of the aligned helices is not well controlled, which results in different angles between the helices and the vertical direction of the CD measurements, and consequent bisignate CD effects similar to those induced by vortex flow in the cuvette in the reference.^[13] The phenomenon has already been observed for the C₃ symmetric P-7-3 molecules, and similar behavior observed for different BTA molecules with assorted defects suggests chirality of all the assemblies. However, the CD profile varies for distinct molecules, indicating deviation of the chiral properties and hence the helical assemblies. In combination, the results of WAXS and CD analyses confirm helical assemblies based on π - π stacking and hydrogen bonding for all BTA molecules similar to the reported P-7-3 molecules. In contrast to the previously reported molecules, which differ merely with respect to the end-groups and assemble with almost identical molecular stacking fashion,^[8] the present molecules deviate much more from P-7-3, so that some modification in the molecular stacking details is not surprising.

The aggregation behavior of the assembled helices and the hierarchical structure in the solution was investigated further by using SAXS (see Figure S3 in the Supporting Information). At sufficiently high concentration, the scattered intensity profiles of BTA molecules show sharp diffraction peaks, an example of which is shown in Figure 3a. An explicit 2D hexagonal structure is observed for the symmetric P-7-3 molecules with the ratio of peak positions of approximately 1: $\sqrt{3}$:2 (Figure 3b), which is attributed to the long-range ordering or hexagonal packing of the supramolecular helices.^[8] The SAXS curves of P-6-2-C, P-7-2-C, and P-8-3 exhibit a broadening of the principle peak (10) and a plateau at high q , which might be composed of smeared higher order peaks, indicating a less well ordered hexagonal symmetry or weaker long-range correlation between helices assembled by defective BTA molecules. All the SAXS profiles can be fitted with hexagonal structures as

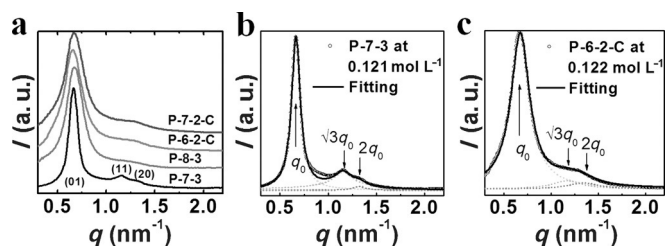


Figure 3. a) Representative SAXS profile for the lyotropic systems of BTA molecules. The concentration was 0.121, 0.122, 0.118, and 0.117 mol L⁻¹ for P-7-3, P-6-2-C, P-7-2-C, and P-8-3, respectively. b) and c) multiple peak fitting of the SAXS with Lorentz shape for P-7-3 and P-6-2-C in (a) reveals hexagonal bundling of the supramolecular assemblies.

shown in Figure 3c, the common hexagonal packing and subsequent interdigitation of neighboring helices contribute to the macroscopic-length scale alignment of the helices observed by CD for the achiral BTA molecules.

With the hexagonal structures, the electron-density profile of aqueous solutions of BTA molecules can be reconstructed from the SAXS patterns (see the Supporting Information for details of the methods used). Figure 4 displays examples of

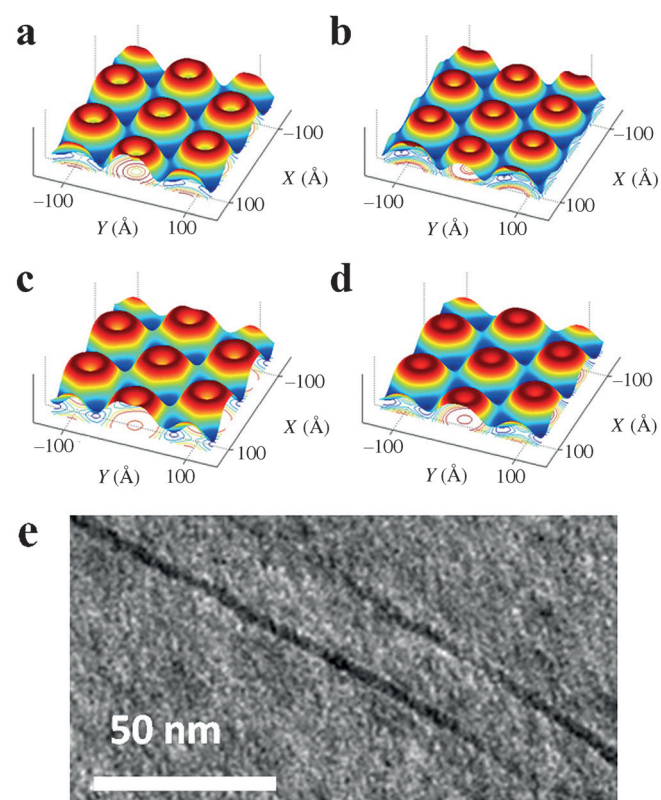


Figure 4. Electron-density profile of the 2D unit cell for BTA/water systems reconstructed from SAXS data. a) P-7-3 at 0.131 mol L⁻¹, b) P-6-2-C at 0.159 mol L⁻¹, c) P-7-2-C at 0.118 mol L⁻¹, and d) P-8-3 at 0.117 mol L⁻¹. The false color marks high intensity in red and low intensity in blue. e) TEM images showing morphology of supramolecular nanotubes. Dilute solution sample was negatively stained by 2 wt% neutral phosphotungstic acid for 15 min before TEM measurement. The tubular structure filled with the staining agent appears dark in TEM as observed in other supramolecular tubular assemblies.

electron-density profiles of BTA/water mixtures at selected concentrations; the plots reveal a similar hexagonal arrangements of annular cylinders or nanotubes separated by continuous regions of low electron-density (shown in deep-blue) corresponding to a solvent sea of water. The annuli of high density and central cylinders of intermediate density correspond to the helical columns assembled by BTA molecules and the central water channels, respectively, indicating the assembly of structures similar to the helical rosette nanotubes reported previously for P-7-3.^[8] The tubular structure is further demonstrated by TEM as shown in Figure 4e. A diluted solution with a concentration of approximately 2 wt% was used to avoid formation of nanotube bundles and to elucidate the morphology of individual nanotubes. Dark filaments with a diameter of approximately 5 nm were observed, which correspond to the hollow core of the supramolecular nanotubes. Further TEM images and related information can be found in Figure S5 and Figure S6 in the Supporting Information. The exterior and inner diameters of the nanotubes (D_w and D_c) can be estimated by examining the cross-section of the electron-density profile of the 2D unit cell along the x-axis, as shown in Figure 5a and

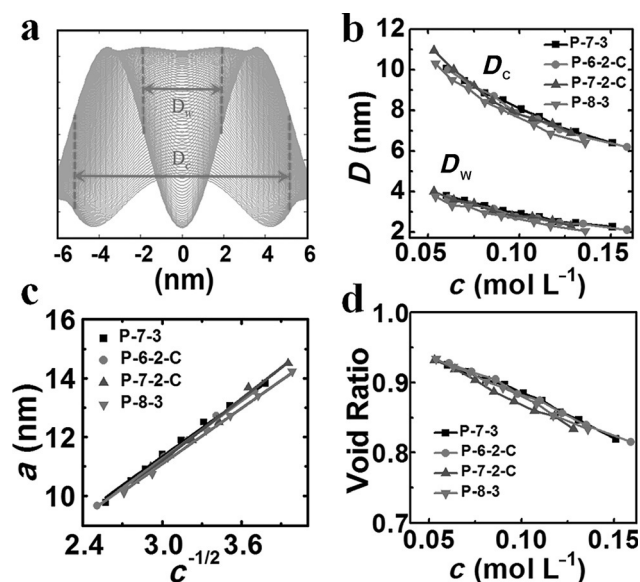


Figure 5. a) A slice along the x axis of the electronic density profile showing the outline of one rosette nanotube and schematic of the diameter of inner water channel (D_w) and exterior annular cylinder (D_c) obtained from the slice. D_w was estimated by the full width at half maximum of the inversed water channel profile and D_c by the separation between the two medium points of the peripheral density profile. b) Change of D_w and D_c with concentration for all BTA molecules; the lines connecting the data points serve as guidance. c) Spacing between adjacent helices, a , calculated from the principle peak position of SAXS versus mole concentration c of the BTA aqueous solutions. The lines are linear fitting of the experimental data. d) Void ratio (volume ratio of the walls not occupied by molecules) calculated with the parameters derived from SAXS.

summarized in Figure 5b. Both diameters decrease with increasing concentration but maintain a gap of approximately 6 nm, which roughly doubles the diameter (3 nm) of the BTA molecules. This suggests that the annular wall is composed of

multiple moieties of BTA molecules arranged shoulder to shoulder along the azimuth, as also observed for **P-7-3**.

The exact number of molecules per stacking layer (N_L) can be derived from the linear fitting of the inter-cylinder separation a or the lattice constant of hexagonal packing as a function of concentration (details of the calculation are given in the Supporting Information), as shown in Figure 5c and summarized in Table 2. Upon dilution, a increases linearly with the

Molecule notation	P-7-3	P-8-3	P-6-2-C	P-7-2-C
number of molecules per layer (N_L)	2.58	2.12	3.06	2.91
number of charged groups per molecule	3	3	2	2
number of charges per layer (N_C)	7.74	6.36	6.12	5.82

square root of concentration, $c^{-1/2}$, expected for expansion of 1D objects in two dimensions. Although a follows a similar trend with very close slope of linearity between 3.2 and 3.5 for all the molecules (see Table S5 in the Supporting Information), N_L deviates because it is determined by both the slope and the molecular weight (which is in contrast to the molecules studied previously because the change in molecular weight is much smaller). The values of N_L span between two and three and show strong dependence on the number of charged groups on the BTAs. The annual cross-section can accommodate approximately three molecules for **P-7-2-C** and **P-6-2-C** with only two charged groups, whereas the occupancy drops for those with three charged groups apparently due to stronger electrostatic repulsion between the molecules. In addition, a more bulky arm of **P-8-3** further suppresses N_L to at most two. The arm length also plays a role in the accommodation of BTA molecules because, in general, N_L decreases with arm length. The above information is in line with WAXS and CD data, which show that the molecular stacking details differ for the BTAs with varied structures.

The hierarchical assemblies of all molecules share very similar structures and geometries, particularly on the nanometer scale. Both the diameters of the helices (2–10 nm) and inter-helices separation (ca. 10 nm) overlap rather well, as shown in Figure 5b–c, manifesting the robust and universal architecture of the assembled helical nanotubes by the fully rigid ionic BTAs despite discrepancies between the molecular details. The stable assembly in water is attributed to the synergy of various noncovalent interplays between the molecules, which demonstrates not only tolerance to ionic defects as previously reported^[8] but also to certain geometric perturbations and even to the coalescence of the two types. The moiety-independent dimensions of supramolecular nanotubes might lead to similar macroscopic properties for different BTAs. As an example, the void ratio of the rosette nanotube (the vacancy of the annular wall) is estimated as described in Figure S7 and Figure S8 in the Supporting Information and plotted in Figure 5d. Despite the differences in N_L (Table 2) and molecular sizes, all BTA molecules give similar values for the void ratio, with minor diver-

gence in the wide range of studied concentrations. The coincidence of the void ratio could be understood by the compensation between N_L and arm length. As mentioned above, N_L decreases with arm length, resulting in roughly the same total volume (N_L multiples the volume of a monomer) occupied by various BTA molecules. The accommodation of molecules inside the supramolecular nanotubes seems to be able to self-adjust to retain the sizes of the rosette nanotubes according to the geometry of each BTA molecule. The estimation is limited by the unknown configuration of the molecules inside the aggregates because the geometry of the molecules are obtained from GaussianView for monomers. Thus, although the values of the void ratio are not exact, they can still serve as a reference for the real system because the change in length should be relatively small for rigid arms. This demonstrates the potential application of this series of molecules as smart materials when molecular functionalization and precise control of sizes or certain macroscopic properties are simultaneously required.

Although the ionic BTA molecules can maintain the hierarchical assembly and bundling of rosette nanotubes very well, divergence does exist in their aggregation behavior. Indeed, although the hexagonal arrays display very similar lattice constant a , the ordering of the arrays varies as indicated by the difference in peak broadening at similar mole concentration in Figure 3a. Compared with **P-7-3**, the disruption of long-range ordering in the assemblies by **P-6-2-C**, **P-7-2-C**, and **P-8-3** can be seen by the broadening of the principle peak as well as by the merging of high-order peaks. To investigate the aggregation thermodynamics further, more detailed analysis of the SAXS was performed to evaluate the principle peak breadth w (full width at half maximum, FWHM) by fitting the principle peak with Pearson type VII function and the higher order peaks with Lorentzian functions. The Pearson function provides an additional free parameter κ and reduces to Lorentzian for $\kappa = 1$.^[14] The use of the Pearson function instead of Lorentzian for peak fitting results in better overall fitting and enables further line broadening analysis.^[15] Figure 6a depicts the change of w with concentration for all BTA molecules, exhibiting qualitatively distinctive behaviors. Whereas w drops for the two molecules with three charged arms, the others with only two

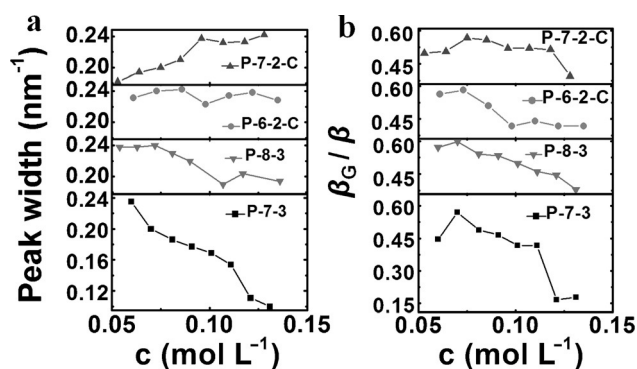


Figure 6. a) FWHM of the principle peak w obtained by fitting the SAXS data with Pearson function and b) calculated broadening from micro-strain (lattice distortion) β_c/β versus mole concentration c .

charged arms show rather slow decrease of w and even the opposite. Interestingly, the decrease of w strongly correlates with the number of charges per layer N_c (equal to N_L times charge on the monomer) given in Table 2. A prominent decrease of w was observed for **P-7-3** with $N_c=7.74$, whereas only a moderate decrease was observed for **P-8-3**, with $N_c=6.36$. For even small N_c , w either decreases only slightly or fluctuates as concentration goes up. With the lowest N_c of less than six, either an increase in w or broadening with concentration instead is observed for **P-7-2-C**.

The width of scattering peaks in liquid crystals is usually related to the long-range ordering of the packing units or correlation length. Generally speaking, the correlation length increases with concentration of the packing units and narrowing of peak width is expected, which is indeed observed for the most charged **P-7-3** assemblies and also for **P-8-3**, albeit to a lesser extent. Then the broadening of the peaks for **P-7-2-C** becomes intriguing. Similar disordering at higher densities was also discovered in DNA packing, which has been attributed to increasing frustration of the molecules.^[16] However, this argument may not apply in our case for two reasons. First, the separation between the supramolecular nanotubes of approximately 10 nm is larger than that between DNA molecules, with an axle–axle distance approximately 3.5 nm. Second, the supramolecular nanotubes are not as rigid as DNA helices and could accommodate a larger number of defects inside the nanotubes while maintaining the long-range positional ordering. The argument that distortion may not account for the broadening observed in this study is further supported by quantitative analysis of the broadening of the principle peak. As an extension of the Voigt function, the Pearson function also allows double Voigt analysis to separate the broadening due to crystalline size (correlation length) and micro-strain (lattice imperfection). The contribution of lattice distortion to the peak broadening (β_c/β) can be estimated by calculating $2w/\beta$ of the principle peak, which gives the value of β_c/β according to reported data.^[15] Here, β stands for integral breadth of the peak and is given in the Supporting Information (Figure S9). As shown in Figure 6b, β_c/β of all lyotropic solutions tend to decrease with molecular concentration after going up slightly at lower concentrations. For asymmetric molecules, the total decrease of β_c/β is of roughly the same magnitude. However the behavior with respect to peak widths is completely different, indicating that peak broadening is not dominated by lattice distortion. Instead, line broadening due to correlation length could be responsible for the distinctive behavior of w .

For the highly charged systems, the driving force for long-range ordered packing could be strong electrostatic repulsion.^[7b] It is not surprising that the correlation length in that case will be dominated by the strength of repulsion. The rapid reduction in peak width w for nanotubes assembled by **P-7-3** could be explained by the promoted long-range ordering with concentration due to stronger repulsion between the nanotubes with the largest number of charged groups. The dramatic suppression of β_c/β also contributes to the peak narrowing for **P-7-3**. Number of charges along the supramolecular nanotubes decreases progressively for **P-8-3**, **P-6-2-C**, and **P-7-2-C**,

generating correspondingly weaker repulsion. Consequently, the growth of the correlation length with concentration is gradually depressed following the same sequence, and peak broadening behaves differently (weak decline, fluctuation, and increase as concentration increases, respectively, for the three molecules) even with similar change of β_c/β . Nevertheless, the behavior of **P-7-3** and **P-8-3** is distinct from that of **P-6-2-C** and **P-7-2-C** in terms of clustering, which is also demonstrated by the difference in POM in Figure S2 in the Supporting Information for the two types of BTA molecules. The apparent stripes observed for **P-7-3** and **P-8-3** indicate well-defined columnar packing, the absence of which in the solutions of **P-6-2-C** and **P-7-2-C** suggests less well ordered columnar arrangements. The contrast between BTA molecules with different numbers of ionic groups demonstrates the subtle influence of surface charge density on the long-range ordering and arrangements of highly charged supramolecular columns.

Conclusion

BTA molecules are more structurally versatile because of the various repeating linkages between the central cores and the peripheral functional groups. Directionality of hydrogen bonds and π – π interactions between the fully rigid BTA molecules cooperating solvophobic effects and electrostatic repulsive interaction^[17] contributes to the stability of the lyotropic liquid-crystal phases. Here, we demonstrate the robustness of supramolecular hierarchical structures with similar stacking architecture and packing behavior for fully rigid ionic BTA molecules with structural versatility along one arm. The mode of molecular stacking, such as the number of molecules per stacking layer, is determined jointly by rigid arm length and the ionic terminals in a way that mesoscopic parameters, including diameters and internanotube distances, can be maintained almost constant for different BTA molecules. The only nuance of long-range ordering is found in terms of correlation length depending on the charge distribution along the nanotubes. The similarity in the dimensions and ordering of the nanotubes assembled by the BTA molecules reflects the robust architecture imparted by synergetic multiple noncovalent interactions. In contrast to the assembly of molecules with flexible chains, which show sensitivity to the geometry and component of the arm,^[18] fully rigid ionic BTA molecules can self-assemble into hierarchical structures with excellent control over geometry and symmetry on the nanometer scale. As a result, it is possible to regulate supramolecular structures for new functional materials by modulating the functional group distribution, hydrophobic arm numbers, and arm length without losing the hierarchical architecture of the assembly. In addition, the sensitivity of aggregation to the chemical and geometrical structures of the BTA molecules demonstrated here can help understand the subtleties involved in hierarchical supramolecular assembly. This knowledge can be used for the design and construction of more complex lyotropic mesogenic structures.

Experimental Section

POM was acquired with an Olympus (Japan) BX-51-P microscope system. CD spectra were recorded with a Jasco U-810 spectropolarimeter. A drop from the sample solution was added between two silicon glass plates that were then sheared several times to obtain a homogeneous thin film of sample. The above sample preparation can solve the problem of saturation that is presented by using a cuvette. However, shear may introduce random orientation of the assembled helices and subsequent artificial contribution in the CD, as discussed in the main text. SAXS measurements were carried out at beamline 16B1 in the Shanghai Synchrotron Radiation Facility. The X-ray wavelength used was 0.124 nm, and a Mar165 CCD detector (2048×2048 pixels with a pixel size of 80 μm) was employed to collect 2D SAXS patterns with sample-to-detector distances of 2025 mm. WAXS measurements were carried out at beamline 1W2A in the Beijing Synchrotron Radiation Facility with wavelength of 0.154 nm and sample-to-detector distance of 145 mm. The sample cell with aqueous solutions sealed between two Kapton membranes were fixed on a sample holder during the measurements. Fit2D software from the European Synchrotron Radiation Facility was used to analyze scattering patterns in terms of the scattering vector $q = 4\pi \sin \theta / \lambda$, with 2θ as the scattering angle and λ as the X-ray wavelength. The method used to reconstruct the electron-density profile from X-ray scattering data for columnar phases (2D periodic systems) has been reported previously.^[8]

Acknowledgements

This work is supported by the National Natural Science Foundation of China (51325301, U1232129), the Fundamental Research Funds for the Central Universities (WK2310000049), and the SAXS experiments are carried out at line 16B of the Shanghai Synchrotron Radiation Facility (SSRF) and 1W2A SAXS station at Beijing Synchrotron Radiation Facility (BSRF).

Keywords: nanotubes · noncovalent interactions · self-assembly · supramolecular chemistry · X-ray diffraction

- [1] a) T. Aida, E. W. Meijer, S. I. Stupp, *Science* **2012**, *335*, 813–817; b) D. T. Bong, T. D. Clark, J. R. Granja, M. R. Ghadiri, *Angew. Chem. Int. Ed.* **2001**, *40*, 988–1011; *Angew. Chem.* **2001**, *113*, 1016–1041; c) T. Shimizu, M. Masuda, H. Minamikawa, *Chem. Rev.* **2005**, *105*, 1401–1444.
 [2] a) F. García, P. M. Viruela, E. Matesanz, E. Ortí, L. Sánchez, *Chem. Eur. J.* **2011**, *17*, 7755–7759; b) F. Wang, M. A. J. Gillissen, P. J. M. Stals, A. R. A. Palmans, E. W. Meijer, *Chem. Eur. J.* **2012**, *18*, 11761–11770.
 [3] a) S. Cantekin, T. F. de Greef, A. R. Palmans, *Chem. Soc. Rev.* **2012**, *41*, 6125–6137; b) B. P. Dash, R. Satapathy, E. R. Gaillard, J. A. Maguire, N. S.

- Hosmane, *J. Am. Chem. Soc.* **2010**, *132*, 6578–6587; c) L.-L. Lai, S.-J. Hsu, H.-C. Hsu, S.-W. Wang, K.-L. Cheng, C.-J. Chen, T.-H. Wang, H.-F. Hsu, *Chem. Eur. J.* **2012**, *18*, 6542–6547.
 [4] a) J. Lydon, *Curr Opin Colloid Interface Sci* **2004**, *8*, 480–490; b) J. Lydon, *J. Mater. Chem.* **2010**, *20*, 10071; c) S.-W. Tam-Chang, L. Huang, *Chem. Commun.* **2008**, 1957.
 [5] a) M. Lehmann, *Chem. Eur. J.* **2009**, *15*, 3638–3651; b) M. Lehmann, M. Jahr, F. C. Grozema, R. D. Abellon, L. D. A. Siebbeles, M. Müller, *Adv. Mater.* **2008**, *20*, 4414–4418.
 [6] a) Y. Huang, Y. Cong, J. Li, D. Wang, J. Zhang, L. Xu, W. Li, L. Li, G. Pan, C. Yang, *Chem. Commun.* **2009**, 7560; b) T. Kato, N. Mizoshita, K. Kishimoto, *Angew. Chem. Int. Ed.* **2006**, *45*, 38–68; *Angew. Chem.* **2006**, *118*, 44–74; c) T. Kato, T. Yasuda, Y. Kamikawa, M. Yoshio, *Chem. Commun.* **2009**, 729.
 [7] a) H. Cui, E. T. Pashuck, Y. S. Velichko, S. J. Weigand, A. G. Cheetham, C. J. Newcomb, S. I. Stupp, *Science* **2010**, *327*, 555–559; b) L. C. Palmer, C. Y. Leung, S. Kewalramani, R. Kumthekar, C. J. Newcomb, M. Olvera de La Cruz, M. J. Bedzyk, S. I. Stupp, *J. Am. Chem. Soc.* **2014**, *136*, 14377–14380.
 [8] D. Wang, Y. Huang, J. Li, L. Xu, M. Chen, J. Tao, L. Li, *Chem. Eur. J.* **2013**, *19*, 685–690.
 [9] J. van Herikhuyzen, P. Jonkheijm, A. P. H. J. Schenning, E. W. Meijer, *Org. Biomol. Chem.* **2006**, *4*, 1539.
 [10] a) V. Percec, A. E. Dulcey, M. Peterca, M. Ilies, S. Nummelin, M. J. Sienkowska, P. A. Heiney, *Proc. Natl. Acad. Sci. USA* **2006**, *103*, 2518–2523; b) V. Percec, A. E. Dulcey, V. S. K. Balagurusamy, Y. Miura, J. Smidrkal, M. Peterca, S. Nummelin, U. Edlund, S. D. Hudson, P. A. Heiney, H. Duan, S. N. Magonov, S. A. Vinogradov, *Nature* **2004**, *430*, 764–768.
 [11] a) J. K. Hirschberg, L. Brunsveld, A. Ramzi, J. A. Vekemans, R. P. Sijbesma, E. Meijer, *Nature* **2000**, *407*, 167–170; b) A. Pawlik, S. Kirstein, U. De Rosi, S. Daehne, *J. Phys. Chem. B* **1997**, *101*, 5646–5651.
 [12] S. Park, B. K. Cho, *Soft Matter* **2015**, *11*, 94–101.
 [13] a) M. Wolffs, S. J. George, Z. Tomovic, S. C. J. Meskers, A. P. H. J. Schenning, E. W. Meijer, *Angew. Chem. Int. Ed.* **2007**, *46*, 8203–8205; *Angew. Chem.* **2007**, *119*, 8351–8353; b) A. Tsuda, M. A. Alam, T. Harada, T. Yamaguchi, N. Ishii, T. Aida, *Angew. Chem. Int. Ed.* **2007**, *46*, 8198–8202; *Angew. Chem.* **2007**, *119*, 8346–8350.
 [14] E. Grelet, *Phys. Rev. Lett.* **2008**, *100*, 168301.
 [15] J. I. Langford, *J. Appl. Crystallogr.* **1978**, *11*, 10–14.
 [16] H. Strey, J. Wang, R. Podgornik, A. Rupprecht, L. Yu, V. Parsegian, E. Sirota, *Phys. Rev. Lett.* **2000**, *84*, 3105.
 [17] a) D. L. Gin, W. Gu, B. A. Pindzola, W.-J. Zhou, *Acc. Chem. Res.* **2001**, *34*, 973–980; b) A. R. A. Palmans, E. W. Meijer, *Angew. Chem. Int. Ed.* **2007**, *46*, 8948–8968; *Angew. Chem.* **2007**, *119*, 9106–9126; c) P. J. M. Stals, J. C. Everts, R. de Bruijn, I. A. W. Filot, M. M. J. Smulders, R. Martín-Rapún, E. A. Pidko, T. F. A. de Greef, A. R. A. Palmans, E. W. Meijer, *Chem. Eur. J.* **2010**, *16*, 810–821.
 [18] a) M. M. Smulders, A. P. Schenning, E. Meijer, *J. Am. Chem. Soc.* **2008**, *130*, 606–611; b) J. J. van Gorp, J. A. Vekemans, E. Meijer, *J. Am. Chem. Soc.* **2002**, *124*, 14759–11476.

Received: April 12, 2015

Published online on September 2, 2015